Title

Shared-photodetector readout to improve the sensitivity of positron emission tomography

Journal

Physics in Medicine and Biology, 63(20)

ISSN

0031-9155

Authors

Du, Junwei
Peng, Peng
Bai, Xiaowei
et al.

Publication Date

2018-10-01

DOI

10.1088/1361-6560/aae056

Peer reviewed

HHS Public Access

Author manuscript

Phys Med Biol. Author manuscript; available in PMC 2019 October 09.

Published in final edited form as:

Phys Med Biol. ; 63(20): 205002. doi:10.1088/1361-6560/aae056.

Shared-Photodetector Readout to Improve the Sensitivity of PET

Junwei Du, **Peng Peng**, **Xiaowei Bai**, and **Simon R. Cherry**

Department of Biomedical Engineering, University of California-Davis, One Shields Avenue, Davis, CA 95616, USA

Abstract

Sensitivity is an important performance characteristic of positron emission tomography (PET) systems. Improved sensitivity can be used to reduce injected dose, reduce scan time, or improve the signal-to-noise ratio and temporal resolution for dynamic studies. One way to improve the sensitivity of PET scanners is to reduce the gaps between detector modules. In this paper, a new signal processing method, named the shared-photodetector readout method, is proposed and evaluated. In this method, the signals generated in nearest neighbor photodetectors adjacent to the detector module of interest, were used to help identify the interaction location in the detector module of interest. Using this method, scintillator arraybased detector modules with almost 100% packing fraction can be built, and the edge crystals can be clearly resolved, even when the crystals are small compared to the photodetector size. To evaluate this signal processing concept in one dimension, a detector block with four dual-ended readout detector modules, was designed. The detector block consisted of eight 4 × 4 arrays of SensL MicroFJ-30035 SiPMs coupled to both ends of a 14 × 56 array of 0.9 × 0.9 × 20 mm^3 LYSO elements with a pitch size of 0.96 mm and a length of 20 mm. Performance in terms of energy resolution, flood histogram, timing resolution and depth-of-interaction resolution obtained using the shared-photodetector readout method were compared to those obtained using a conventional readout method. The results show that better over-all performance was achieved using the shared-photodetector readout method, especially at the edges and corners of the array.

1 Introduction

Sensitivity is an important characteristic defining the performance of positron emission tomography (PET) systems. Improved sensitivity can be used to reduce injected dose, reduce scan time, or perhaps most importantly, improve the signal-to-noise ratio and temporal resolution for dynamic studies (Cherry *et al* 2018). During the past several decades, the sensitivity of PET has been greatly improved, however, it is still a limiting factor in many studies (such as dynamic studies) and is far from what is theoretically possible. Different methods have been proposed to improve the sensitivity or effective sensitivity of PET (Wong 1993, St James *et al* 2010, Surti 2014, Vinke and Levin 2014 and González-Montoro *et al* 2017). The sensitivity can be improved using thicker or more efficient scintillator, increasing solid angle coverage, or reducing deadspace/gaps within and between detector modules (St James *et al* 2010 and Cherry *et al* 2018). Very significant improvements are possible by

jwdu@ucdavis.edu.

addressing all these factors. The vast majority of PET studies, especially dynamic studies, are count-limited and would benefit tremendously from significant gains in detection sensitivity.

Most human PET scanners use scintillator elements with a length longer than 18 mm. While some gains can be realized by using longer scintillators, this is not very cost-effective due to the exponential drop in absorption with depth of the gamma photons in the scintillator (Cherry *et al* 2012). However, the sensitivity can still be greatly improved by reducing the gaps/dead space between scintillator elements and detector modules (St James *et al* 2010 and González-Montoro *et al* 2017). PET detectors based on monolithic crystals, which eliminate the dead space caused by the reflectors in scintillator arrays, have been successfully used for preclinical PET and are under evaluation for clinical PET (Pajak *et al* 2016 and Mikhaylova *et al* 2017). However, the readout electronics and position estimation algorithms are more complicated and require very careful calibration compared to PET detectors based on scintillator arrays, which typically use simple center of gravity algorithms to estimate the gamma photon interaction position (Joung *et al* 2002, Wang *et al* 2011 and Du *et al* 2016). Furthermore, the resolution obtained from PET detectors based on thick monolithic scintillators are not in general as good as these obtained from PET detectors based on scintillator arrays (Borghi *et al* 2018 and Du *et al* 2018).

To obtain uniform resolution across the field of view (FOV), PET detector modules with depthof-interaction (DOI) information are required. PET detectors based on dual-ended readout method have been demonstrated to have excellent DOI resolution (Yang *et al* 2009 and Du *et al* 2018). Figure 1 (top row) shows a schematic of a PET scanner based on detectors with dual-ended readout using silicon photomultipliers (SiPMs). The gaps between detector modules significantly reduce the sensitivity of the PET scanner. Due to the truncation of the light distribution at the edges of the detector modules, the only way to resolve all the elements in the scintillator array when the crystal size is less than the SiPM dimensions is to make the scintillator array smaller than the SiPM array (Yamamoto *et al* 2013 and Du *et al* 2016). This results in a low packing fraction and makes the gaps between the detector modules even larger. Tapered scintillator array and position-sensitive APDs or position- sensitive SiPMs have been used to reduce the gaps, but the gaps are not eliminated (Yang *et al* 2009 and Du *et al* 2018).

We plan to build a scanner for human brain studies without gaps between detector modules based on identical tapered scintillator elements (figure 1 (bottom)). In this scanner, all the crystals face the center of the FOV in the transaxial plane (making the system highly symmetric) and the only dead space is the 60–70 μm thick reflector used between the scintillator elements. The sensitivity of the proposed scanner can be increased by more than a factor of two compared with the conventional design. To resolve the scintillator elements coupled to the edge of the SiPM arrays, a shared-photodetector readout method that incorporates the signals from neighboring SiPMs will be used.

In this paper, the shared-photodetector readout method was evaluated in simplified one dimensional version using a detector block consisting of four rectangular dual-ended readout detector modules. The performance (energy resolution, flood histogram, timing resolution

and DOI resolution) of the detector block was evaluated and compared using both the shared-photodetector readout method and the conventional readout method. Particular attention was paid to the performance measured in crystals at the interfaces between the four modules.

2 Materials and Methods

2.1. DOI detector block

The DOI detector block (figure 2 (bottom)) consists of two pre-amplifier boards (figure 2 (top left)) and a 14 × 56 array of 0.90 × 0.90 × 20 mm3 polished LYSO crystals (figure 2 (top right)). The pitch size of the LYSO array is 0.96 mm and Toray is used as the reflector between crystals. Previous studies have demonstrated this is an appropriate combination of surface treatment and reflectors to give good positioning, energy resolution and DOI resolution (Ren et al 2014). Each pre-amplifier board holds four 4 × 4 arrays of SensL MicroFJ-30035 SiPMs. The pitch of the SiPMs in the array is 3.36 mm. 53.8 × 13.5 × 1 mm3 clear acrylic sheets were used as light guides and optical grease BC-630 was used as the coupling material between the LYSO arrays, the acrylic sheets and the SiPM arrays.

2.2. Shared-photodetector readout method

The output of each SiPM in the 4 × 4 SiPM array was split into two equal parts using two 4.7 nF capacitors (figure 3(top)). The signals in the same row/column are summed together to generate 4 row signals and 4 column signals for each 4 × 4 SiPM array (figure 3 (top)) and then amplified individually using AD8056 amplifiers (Analog Devices, Inc.). The 8 amplified row/column signals from each 4 × 4 SiPM array together with the signal(s) from the neighboring column(s) of SiPMs from the adjacent array were sent to the position encoding board and weighted according to the positions of the SiPMs, generating 4 signals for position information (figure 3 (bottom) and figure 4). For each of the four DOI detector modules with two 4 × 4 SiPM arrays, 8 position signals are generated, and the timing signal is taken as the sum of all the amplified row/column signals. As this DOI detector is made up of four detector modules, 32 signals for position information and 4 signals for timing information are generated. As signals from each SiPM array are shared with its immediate neighbors, we named this readout method the shared-photodetector readout method (abbreviated as SDRM).

In the current detector design, the shared-photodetector readout method was evaluated in just one dimension (x direction), as shown in figure 3 (bottom). In the y direction, as the SiPM arrays do not have neighbors, the conventional readout method is used. The performance of the detector obtained using SDRM was compared to that obtained using the conventional readout method (abbreviated as Conv.) which did not use information from neighboring modules.

2.3. Signal and data processing

The outputs from the SDRM boards (figure 4) or the Conv. boards were fed in to a spectrum amplifier (CAEN 7546B) for further shaping and digitized by a PowerDAQ board (PD2MFS, United Electronic Industries). Since the PowerDAQ board has just 8 input

channels, the four detector modules in the detector block were tested one by one. The PowerDAQ boards were installed in a computer and data were stored in list mode for further processing.

The gamma photon interaction position (x, y), deposited energy (E) and DOI information were calculated as follows:

$$x = \frac{1}{2}\left(\frac{X_1^+ - X_1^-}{X_1^+ + X_1^-} + \frac{X_2^+ - X_2^-}{X_2^+ + X_2^-}\right), y = \frac{1}{2}\left(\frac{Y_1^+ - Y_1^-}{Y_1^+ + Y_1^-} + \frac{Y_2^+ - Y_2^-}{Y_2^+ + Y_2^-}\right) \quad (1)$$

$$\mathrm{E} = \mathrm{E}_1 + \mathrm{E}_2 \quad (2)$$

$$\mathrm{DOI} = a\left(\frac{E_1 - E_2}{E_1 + E_p}\right) + \mathrm{b} \quad (3)$$

where $E_1 = X_1^+ + X_1^- + Y_1^+ + Y_1^-$ and $E_2 = X_2^+ + X_2^- + Y_2^+ + Y_2^-$ were the two energies detected by the two SiPM arrays coupled at opposite ends of the LYSO array. $X_i^+, X_i^-, Y_i^+, Y_i^- (i = 1, 2)$ are the position signals. a and b are constants used to model the relationship between the ratio of the two energies and the DOI. The timing signals of one detector module was fed into constant fraction discriminator (CFD, ORTEC 584) to generate a timing stamp and trigger for the DAQ board.

2.4 Experimental methods

During the experiments, the DOI detector module was located inside a light-tight aluminum enclosure that was connected to ground. The temperature inside the enclosure was controlled at 15 ± 0.5 °C using an air-jet crystal cooler (FTS System, Inc.) and monitored by a Type K thermocouple (DigiSense, Inc.). A bias voltage of 28.0 V was applied to both SiPM arrays coupled to the LYSO array. A 40 uCi ^{22}Na point source with a diameter of 0.25 mm was used to irradiate the LYSO array during all experiments.

For the flood histogram and timing measurements, a Hamamatsu PMT R13349–10 coupled to a 16 × 16 × 16 mm^3 LYSO crystal was used as a reference detector to collect coincidence events. The energy resolution and peak position of the 511 keV gamma photons were extracted using the data obtain for the flood histograms. For the DOI measurements, a reference detector consisting of a 0.5 × 20 × 20 mm^3 LYSO crystal and the same PMT was used to electronically collimate the interaction depth (Du *et al* 2018). The PMT signal was amplified by a transimpedance amplifier (based on AD8045) and then fed in to a CFD (ORTEC 584) for time pick-off. To assign the obtained events to each crystal, a look up table (LUT) was generated from the flood histogram, and then this LUT was applied to the data.

2.4.1 Flood histograms—Figure 5 shows a raw flood histogram of one of the center detector modules generated using the SDRM. As expected, the first few columns of the neighboring modules are also seen because of the signal sharing method. The events belonging to the crystals shown in the white rectangle (which are coupled to this specific detector module) were selected before further processing.

After the data was segmented using the LUT for each crystal, a 350–750 keV energy window was applied to each individual crystal to select events, in order to generate the final energywindowed flood histogram. To quantitatively compare the resulting flood histograms, a quality metric was calculated as the ratio of the distance to the width of the crystal spots corresponding to neighboring crystals in the flood histogram (Du *et al* 2016).

2.4.2 511 keV photopeak position and energy resolution—After the energy spectra were extracted for each crystal in the LYSO array, a Gaussian fit was applied to the photopeak of the energy spectra. The centroid of the Gaussian fit was taken as the photopeak position of the 511 keV photons and the FWHM of the Gaussian fit to its centroid was taken as the energy resolution for this crystal. The average and standard deviation of the energy resolution of all crystals in one detector module were used as a measure of the energy resolution of this detector module.

2.4.3 Timing resolution—Timing spectra were also extracted for each crystal with a 350–750 energy window to select events, and then a Gaussian fit was applied to the timing spectra. The FWHM of the Gaussian fit was taken as the timing resolution with the PMT based reference detector, which has a timing resolution of 548.7 ps.

2.4.4 DOI resolution—The DOI resolution was measured at five depths, ranging from 2 mm to 18 mm, in 4 mm steps (Moses *et al* 1994 and Du *et al* 2018). With a 350 – 750 keV energy window applied to the segmented crystal data to select events, DOI calibration parameters a and b in equation 3 was extracted for each crystal and then the depth information for each event was calculated using equation 3. At each depth, different sets of events were used for the calibration step and for measurement of DOI resolution.

2.4.5 False triggers—Since the signals for edge SiPMs were shared between detector modules (figure 3 (bottom)), it is possible that an event can be detected by more than one detector module. This situation mostly happens when the gamma photons interact at the edge of one detector module, as shown in figure 5. If a gamma photon interacts with detector module A, but a trigger is detected by its neighbor detector module B, the trigger is a false trigger for detector module B. These false triggers will increase the event rate, dead time and pile-up of detector module B. The false trigger issue was studied using one of the center detector modules by investigating the energy spectra.

3. Results

3.1 Flood histograms

Figure 6 shows the flood histograms of the four detector modules obtained using the two readout methods. It is clear that more LYSO elements are identified using SDRM. For the

two center detector modules, which benefit from the SDRM method, all the crystals in the *x* direction can be identified.

Figure 7 (top) shows the normalized position profiles for the seventh crystal row obtained using the two readout methods. 52 of the 56 crystals can be resolved using SDRM, the only ones not resolved are at the extreme edges of Detector 1 and 4 where there are no neighboring detectors and thus SRDM is not applied. For the conventional method only 44 separate peaks are resolved in a row of 56 crystals. To quantitatively compare the flood histograms, flood histogram quality metrics are shown in figure 7 (bottom). For each detector module, the flood histogram quality was calculated using all 14 × 14 crystals or just the central 6 × 6 crystals (Figure 7 (bottom)). When all 14 × 14 crystals are analyzed, due to the fact that the edge crystals cannot be resolved using the Conv. method, the average flood histogram quality is better using SDRM. When using just the central 6 × 6 crystals, which are well resolved with both methods, the Conv. method has a tendency to be slightly better, because the noise using SDRM, which sums signals from more SiPMs, is higher.

3.2 511 keV photopeak position and energy resolution

Figure 8 shows the photopeak position of 511 keV photons for each crystal, whilst the energy resolution is shown in figure 9 (top). In cases where two crystals are not resolved and form a single spot in the flood histogram, the spot is divided and events from the left and right sides are assigned to the two crystals. It is clear that the photopeak position and energy resolution obtained using SDRM is better than that obtained using Conv., especially for crystals at the interface between detector modules, as more light was collected.

The average energy resolution across all crystals for each detector module is shown in figure 9 (bottom). The average energy resolution obtained using SDRM is better than that obtained using Conv. when all crystals were used, and the average energy resolution obtained using the two readout methods are comparable when only the center 6 × 6 crystals were considered.

3.3 DOI resolution

Figure 10 (top) shows the average DOI resolution across the five depths for each crystal obtained using the two readout methods, and figure 9 (bottom) shows the average DOI resolution across all depths and using the 14 × 14 crystals and the central 6 × 6 crystals for each detector module. The average DOI resolution obtained using different readout methods are comparable, indicating the DOI resolution was not greatly affected by the readout method. This is consistent with expectations as the DOI is calculated by the ratio of the two energies detected by the two SiPM arrays coupled to the LYSO array.

3.4 Timing resolution

The timing resolution in coincidence with the PMT based reference detector for each crystal in the LYSO array is shown in figure 11 (top). It is clear that the timing resolution of crystals at the interface between the detector modules obtained using SDRM are better than those obtained using the Conv., as more photons are collected as shown in figure 8. However, the

timing resolution of the central crystals obtained using SDRM were slightly worse than those obtained using Conv., which is caused by the higher noise collected by SDRM.

3.5 False Triggers

Figure 12 (top) shows the global energy spectra obtained using the different readout methods, which were obtained from a center detector module and normalized by the number of counts at 511 keV. It is apparent that using SDRM, more events with low energy were acquired due to light sharing between different detector modules. The triggers caused by the events from the neighboring detector modules will increase the event rate that the electronics of the detector module of interest needs to handle, which increases the deadtime. However, if an appropriate threshold is used, the number of events triggering the electronics can be greatly reduced, as shown in figure 12. At a PET system level, as the interaction positions of the gamma photons are calculated on-line (typically using an FPGA or a DSP) (Goertzen *et al* 2017), the events detected by the LYSO crystals of the detector module can be identified on-line (as shown in figure 5), and the event data transferred to the storage/computer can be significantly reduced, thus minimizing deadtime increases.

4. Discussion

We proposed a new readout method, named the shared-photodetector readout method, to solve the edge effect in PET detector modules consisting of scintillator arrays with a pitch size smaller than the pitch size of the photodetector array. The proposed readout method was evaluated in one dimension using a dual-ended readout detector block consisting of four detector modules based on a 14 × 14 array of LYSOs and 4 × 4 arrays of SiPMs. The LYSO array has a pitch size of 0.96 mm and a length of 20 mm, whilst the SiPM arrays have a pitch size of 3.36 mm, fabricated using SensL MicroFJ-30035-TSV SiPMs.

The flood histogram shows that crystals at the interface between the detector modules can be clearly identified using the shared-photodetector readout method, due to signal sharing with adjacent SiPMs, whereas they could not be identified with the conventional readout method (figure 6). The average energy resolution and the average DOI resolution obtained using the proposed readout method and the conventional readout method are comparable, whilst the energy/DOI resolution of the crystals at the interface of detector module obtained using the proposed method are better than those obtained using the conventional readout method as more photons were collected using the proposed method (figures 8, 9 and 10). The average timing resolution obtained using the conventional readout method is slightly better, whilst the timing resolution of the crystals at the interface of detector module obtained using the proposed method are clearly better (figure 11). Considering the major improvement of the flood histogram (figure 6), we believe on balance that better overall performance can be obtained using the shared-photodetector readout method.

The main advantage of the proposed readout is that PET scanners without gaps between detector modules can be built and the sensitivity of the scanner can be improved by using more scintillator volume without using more photodetectors and electronics. The disadvantage of the proposed readout is that noise from more SiPMs is integrated using a multiplexed readout scheme. For dualended readout detector modules consisting of $N \times N$

SiPM arrays coupled to both ends of the scintillator arrays, noise from $2\times(N+1)\times(N+1)$ SiPMs are collected by the readout electronics of one detector module using the shared-photodetector readout method, while noise from $2\times N\times N$ SiPMs are collected by the readout electronics of that detector module using the conventional readout method. Hence, the incremental ratio of the noise is $1/N$ using the shared-photodetector readout method, compared to that of using the conventional readout method. However, for detector modules based on large-area SiPM arrays (N is large), the noise increment using the shared-photodetector readout method can become quite negligible.

5. Conclusions

A new readout method was proposed and evaluated for simultaneous high-resolution and highsensitivity PET scanners based on dual-ended readout detector modules. The performance of the proposed readout in terms of flood histogram, energy resolution, DOI resolution and timing resolution were evaluated and compared with those obtained using the conventional readout method by using a detector block consisting of four dual-ended readout detector modules. The results show that better overall performance was obtained using the shared-photodetector readout method. Although the proposed readout method was evaluated using a dual-ended readout detector, it can also be applied to single-ended readout detector. The promising results achieved lay the foundation for now extending the method to two dimensions and applying it to LYSO arrays of tapered crystals with curved surfaces (figure 1) that allow annular, gap-less detector rings to be constructed.

Acknowledgements

This work was funded by NIH grant R01 EB019439.

References

Borghi G, Tabacchini V, Bakker R and Schaart D 2018 Sub-3 millimeter, near-200 picosecond TOF/DOIPET imaging with monolithic scintillator detectors in a 70 cm diameter tomographic setup Phys. Med. Biol 10.1088/1361-6560/aad2a6.

Cherry S R, Jones T, Karp J, Qi J, Moses W and Badawi R 2018 Total-body PET: maximizing sensitivity to create new opportunities for clinical research and patient care J. Nucl. Med 57 3–12

Cherry S R, Sorenson J A and Phelps M E 2012 Physics in nuclear medicine 4th (Philadelphia, PA: W B Saunders)

Du J, Bai X, Gola A, Acerbi F, Ferri A, Piemonte C, Yang Y, Cherry S R 2018 Performance of a highresolution depth-encoding PET detector module using linearly-graded SiPM arrays Phys. Med. Biol 63 035035 [PubMed: 29324437]

Du J, Yang Y, Bai X, Judenhofer S, Berg E, Di K, Buckley S, Jackson C and Cherry S R 2016 Characterization of large-area SiPM array for PET applications IEEE Trans. Nucl. Sci 63 8–16 [PubMed: 27182077]

Goertzen A, Shrestha R, Khan M, Stortz G, Bishop D, Kozlowski P, Retière F, Thiessen J, Thompson C, and Sossi V 2017 Data acquisition for a preclinical MR compatible PET insert using the OpenPET platform IEEE Trans. Rad. Plasma Med. Sci 1 495–504

González-Montoro A, Aguilar A, Cañizares G, Conde P, Hernández L, Vidal L, Galasso M, Fabbri A, Sánchez F, Benlloch J and González A 2017 Performance study of a large monolithic LYSO PET detector with accurate photon DOI using retroreflector layers IEEE Trans. Rad. Plasma Med. Sci 1 229–237

Joung J, Miyaoka R and Lewellen T 2002 CMICE: a high resolution animal PET using continuous LSO with a statistics based positioning scheme Nucl. Instrum. Methods Phys. Res. A 489 584–598.

Mikhaylova E, Tabacchini V, Borghi G, Mollet P, D'Hoe E, Schaart D and Vandenberghe S 2017 Optimization of an ultralow-dose high-resolution pediatric PET scanner design based on monolithic scintillators with dual-sided digital SiPM readout: a simulation study Phys. Med. Biol 62 8402–8418 [PubMed: 28944759]

Moses W and Derenzo S 1994 Design studies for a PET detector module using a pin photodiode to measure depth of interaction IEEE IEEE Trans. Nucl. Sci 41 1441–1445.

Pajak M, Volgyes D, Pimlott S, Salvador C, Asensi A, McKeown C, Waldeck J and Anderson K 2016 NEMA NU4–2008 Performance evaluation of Albira: a two-ring small-animal PET system using continuous LYSO crystals Open Med. Jour 3 12–26

Ren S, Yang Y and Cherry S R 2014 Effects of reflector and crystal surface on the performance of a depthencoding PET detector with dual-ended readout Med. Phys 41 072503 [PubMed: 24989406]

St James S, Yang Y, Bowen S, Qi J and Cherry S R 2010 Simulation study of spatial resolution and sensitivity for the tapered depth of interaction PET detectors for small animal imaging Phys. Med. Biol 55 N63–N67 [PubMed: 20023331]

Surti S2014 Update on time-of-flight PET imaging J. Nucl. Med 50 98–105

Vinke R and Levin C 2014 A method to achieve spatial linearity and uniform resolution at the edges of monolithic scintillation crystal detectors Phys. Med. Biol 59 2975–2995 [PubMed: 24841984]

Wang Y, Du J, Zhou Z, Yang Y, Zhang L and Peter B 2011 FPGA based electronics for PET detector modules with neural network position estimators IEEE Trans. Nucl. Sci 58 34–42.

Wong W 1993 A positron camera design with cross-coupled scintillators and quadrant-sharing photomultipliers IEEE Trans. Nucl. Sci 40 962–966

Yamamoto S, Yeom J, Kamada K, Endo T and Levin C S 2013 Development of an ultrahigh resolution block detector based on 0.4 mm pixel Ce:GAGG scintillators and a silicon photomultiplier array IEEE Trans. Nucl. Sci 60 4582–4587

Yang Y et al. 2016 A prototype high-resolution small-animal PET scanner dedicated to mouse brain imaging J. Nucl. Med 57 1130–1135 [PubMed: 27013696]

Yang Y, Qi J, Wu Y, St. James S, Farrell R, Dokhale P, Shah Kand Cherry SR 2009 Depth of interaction calibration for PET detectors with dual-ended readout by PSAPDs Phys. Med. Biol 54 433–445 [PubMed: 19098356]

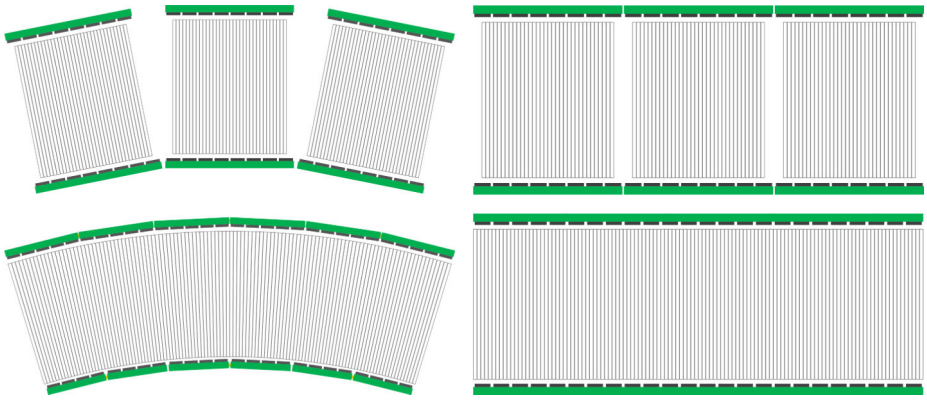

Figure 1.

Schematic of detector module arrangement for (top row) the conventional and (bottom row) the proposed PET scanner based on dual-ended readout method and SiPM arrays. (Left) transverse view and (right) axial view. This figure shows just a part of the whole scanner.

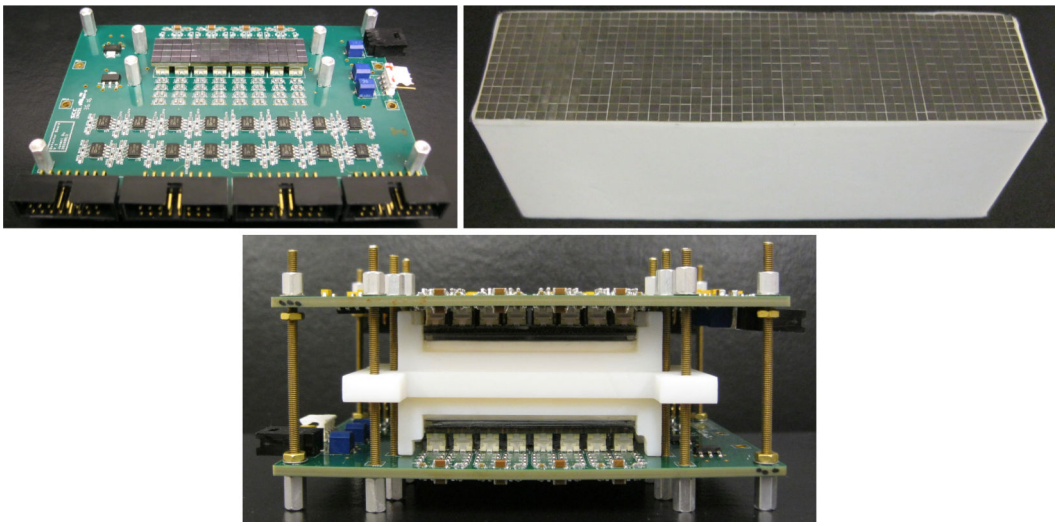

Figure 2.
Photographs of (top left) pre-amplifier board with four SiPM arrays, (top right) the 14 × 56 array of LYSO elements, (bottom) the assembled DOI detector module.

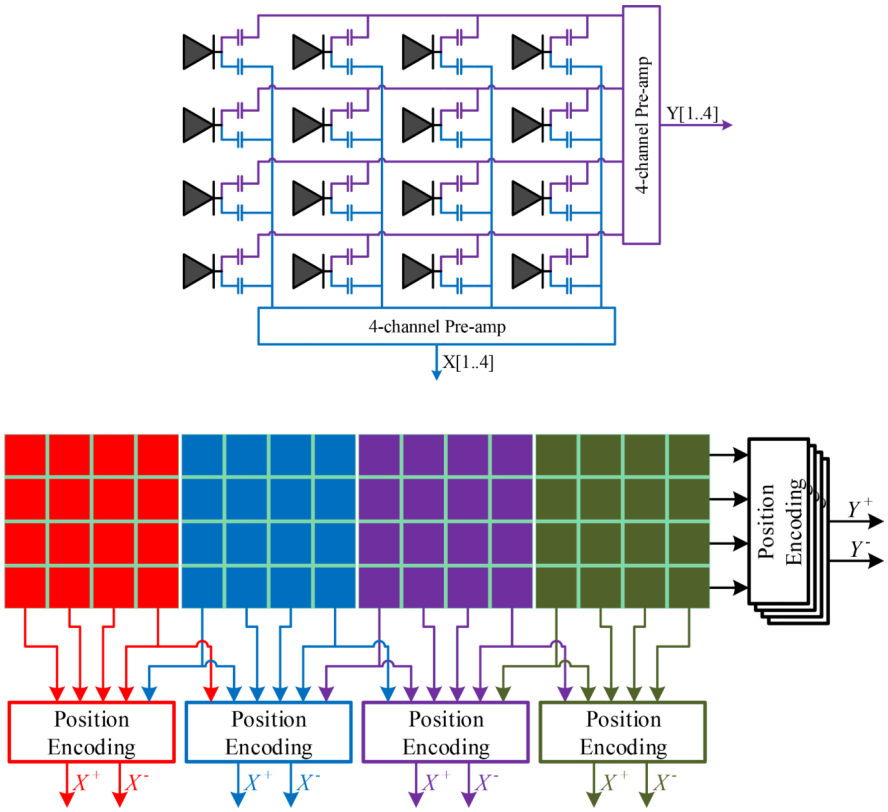

Figure 3.

Schematic of (top) the row and column readout method and (bottom) the one-dimensional shared-photodetector readout method that uses signals from adjacent columns of SiPMs

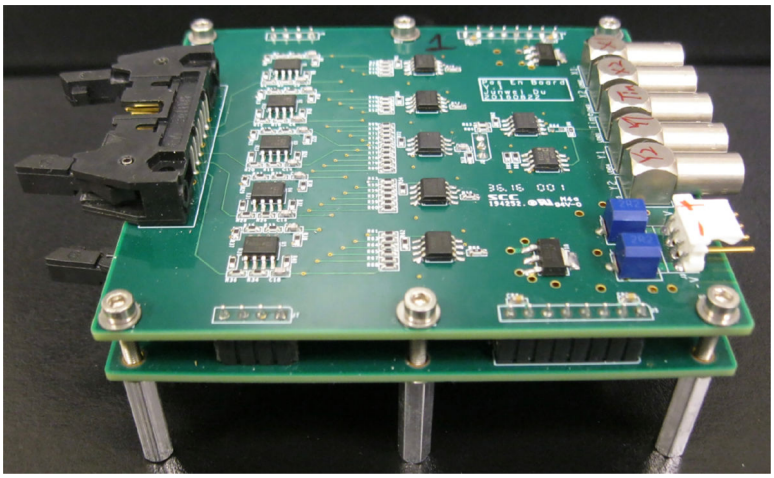

Figure 4.

Photograph of two boards implementing the SDRM for one detector module. Each detector module has its own board. SDRM and Conv. were implemented on the same physical board populated with different components.

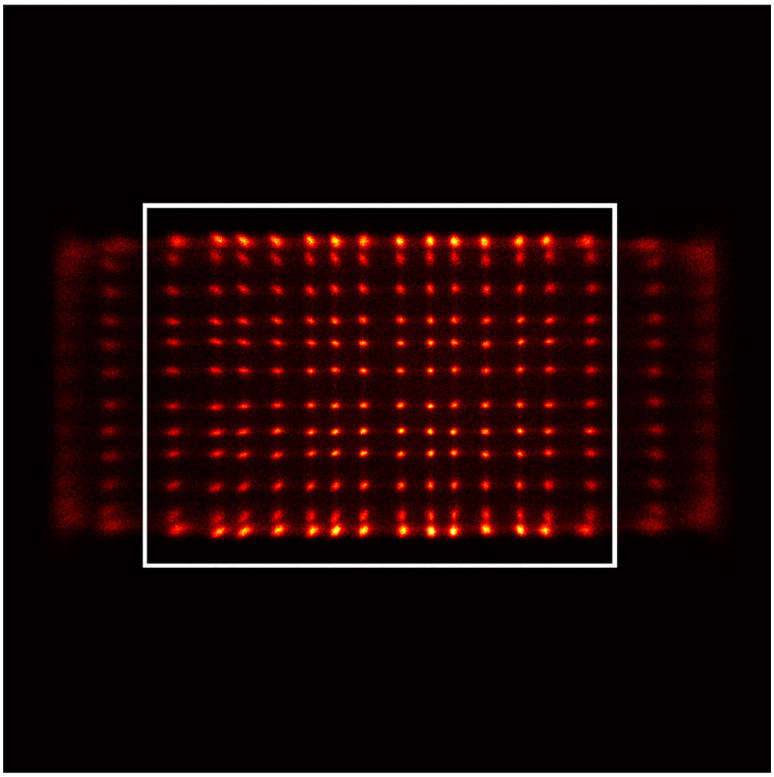

Figure 5.
Raw flood histogram obtained using the SDRM for one center detector module. The white box encompasses the crystals in the detector module of interest.

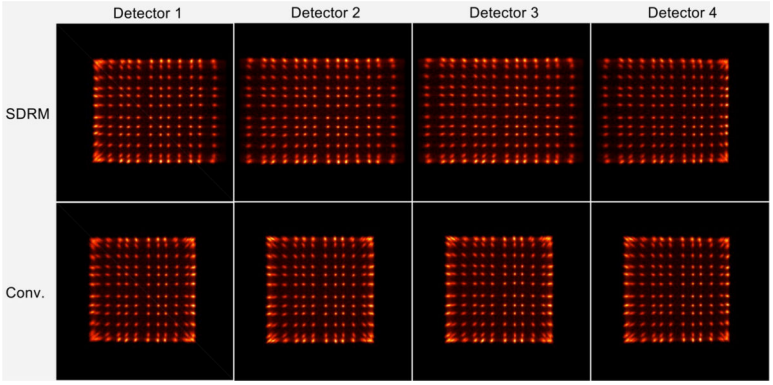

Figure 6.
Flood histograms obtained using the two different readout methods.

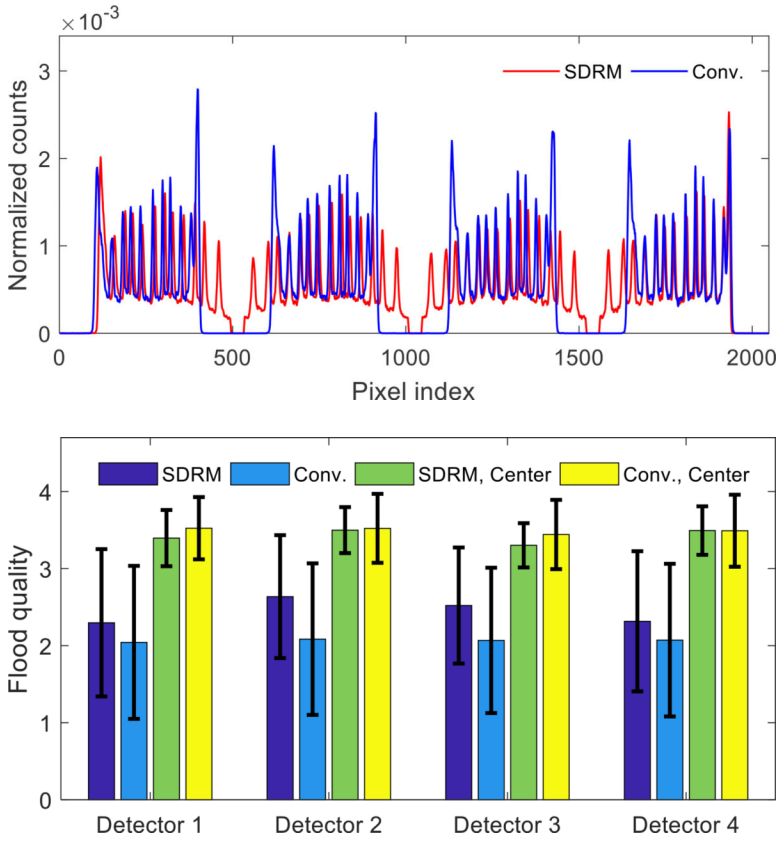

Figure 7.
(top) position profiles and (bottom) flood histogram quality obtained using different readout methods.

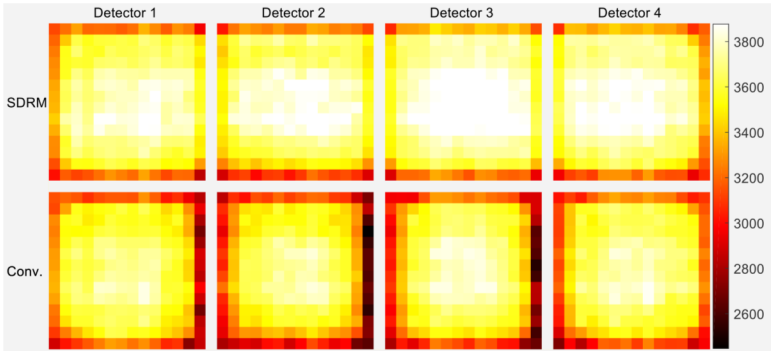

Figure 8.
Photopeak position (amplitude) for each crystal obtained using the two different readout methods.

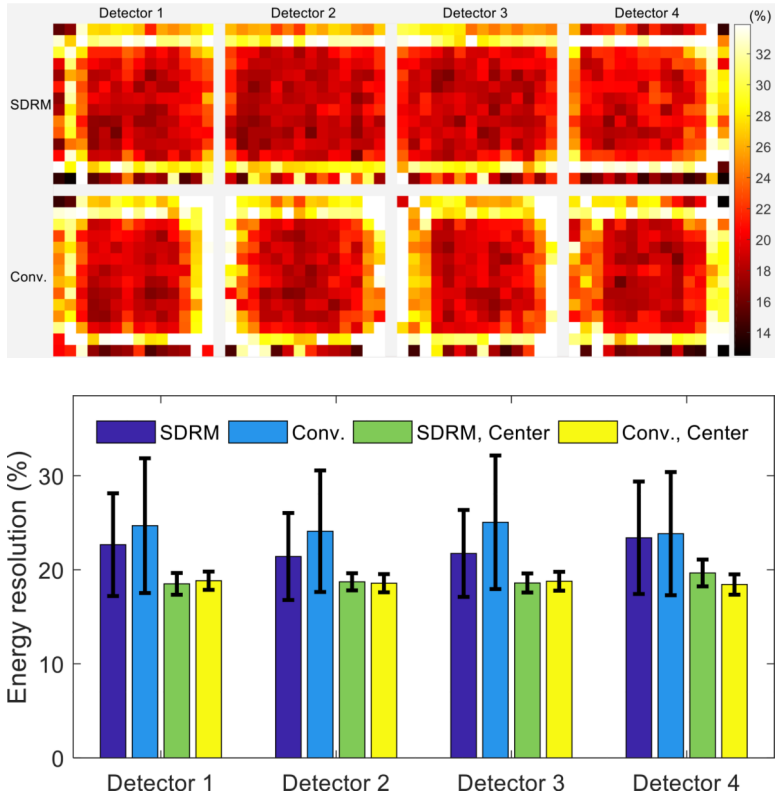

Figure 9.

(top) energy resolution for each crystal obtained using the two different readout methods, and (bottom) average energy resolution for each detector module obtained for the entire array or the central 6 × 6 crystals for both readout methods.

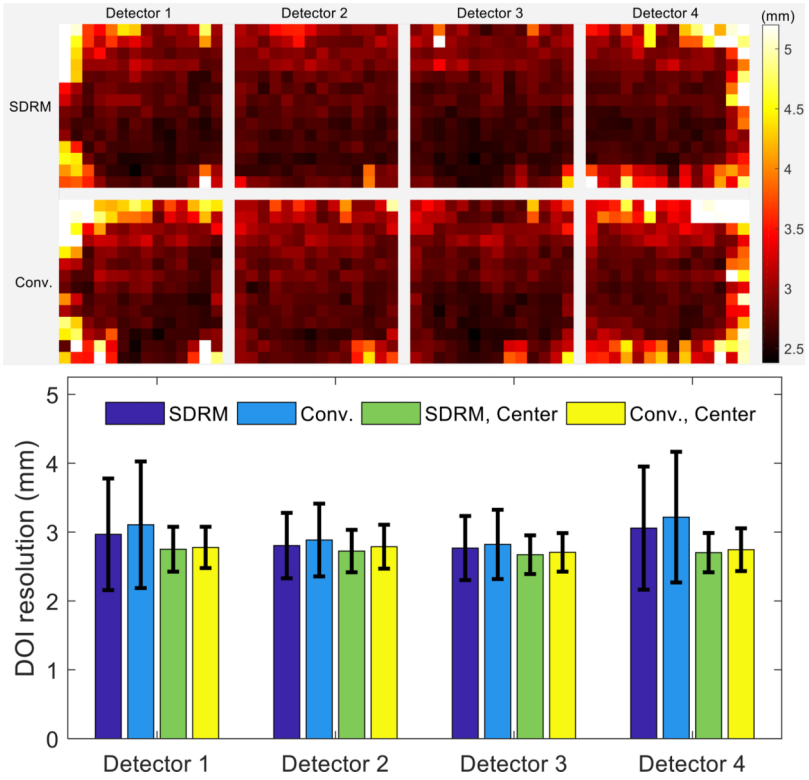

Figure 10.

(top) DOI resolution across the five depths for each crystal obtained using the two different readout methods and (bottom) average DOI resolution across all the depths using all 14 × 14 crystals and the selected center 6 × 6 crystals for each detector module.

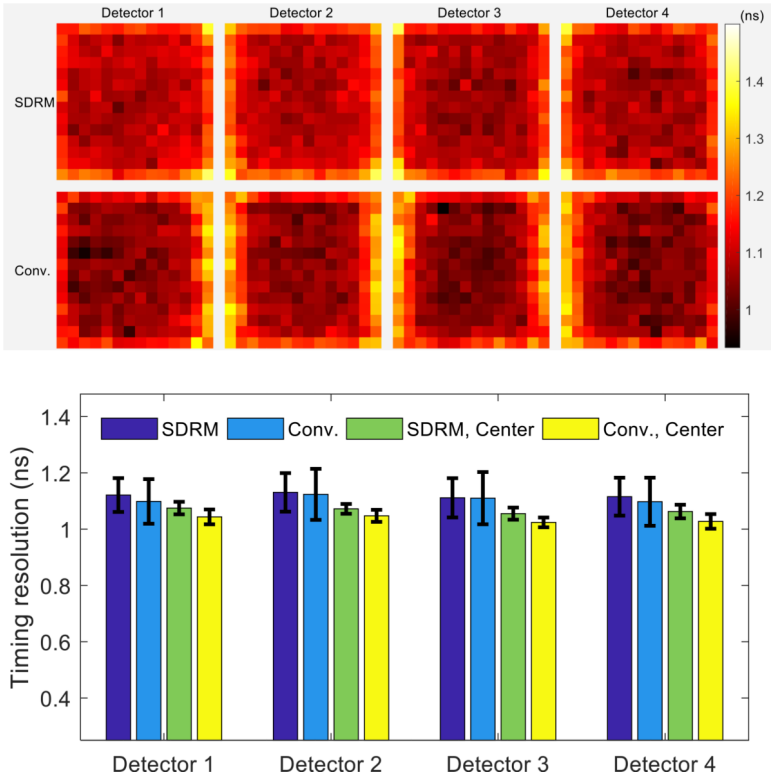

Figure 11.
(top) timing resolution for each crystal in the LYSO array, and (bottom) average timing resolution for each detector module.

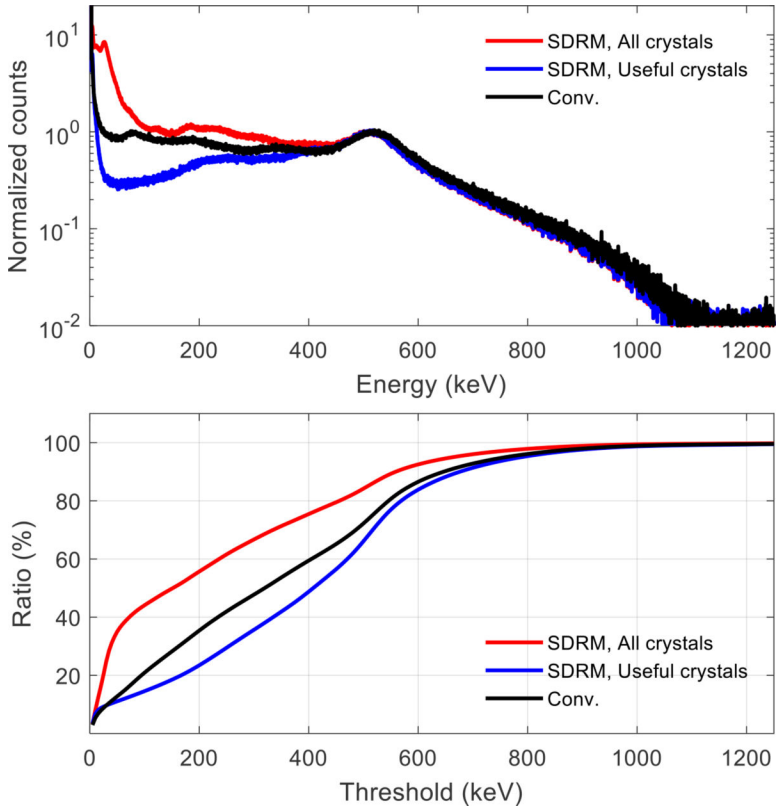

Figure 12.

(top) energy spectra (logarithmic scale) and (bottom) event ratio for events below a given energy threshold obtained using the two different readout methods. “SDRM, All crystals” means that all the events detected by the detector module were used and “SDRM, Useful crystals” means only the events detected by the LYSO crystals coupled to the detector module (as shown in figure 5) were used.